6362 J. Med. Chem. 2009, 52, 6362–6368
DOI: 10.1021/jm900630q

Journal of Medicinal Chemistry Article

Structure-Guided Design of Potent and Selective Pyrimidylpyrrole Inhibitors of Extracellular Signal-Regulated Kinase (ERK) Using Conformational Control†

Alex M. Aronov,* Qing Tang, Gabriel Martinez-Botella, Guy W. Bemis, Jingrong Cao, Guanjing Chen, Nigel P. Ewing, Pamella J. Ford, Ursula A. Germann, Jeremy Green, Michael R. Hale, Marc Jacobs, James W. Janetka, Francois Maltais, William Markland, Mark N. Namchuk, Suganthini Nanthakumar, Srinivasu Poondru, Judy Straub, Ernst ter Haar, and Xiaoling Xie

Vertex Pharmaceuticals Inc., 130 Waverly Street, Cambridge, Massachusetts 02139-4242

Received May 13, 2009

The Ras/Raf/MEK/ERK signal transduction, an oncogenic pathway implicated in a variety of human cancers, is a key target in anticancer drug design. A novel series of pyrimidylpyrrole ERK inhibitors has been identified. Discovery of a conformational change for lead compound **2,** when bound to ERK2 relative to antitarget GSK3, enabled structure-guided selectivity optimization, which led to the discovery of **11e**, a potent, selective, and orally bioavailable inhibitor of ERK.

Introduction

Activation of the Ras/Raf/MEK/ERK[a] signal transduction pathway has been observed in numerous tumor types. This pathway controls a number of fundamental cellular processes including cell survival, proliferation, motility, and differentiation, and its constitutive activation has been reported in lung, colon, pancreatic, renal, and ovarian cancers.[1−5] Extracellular signal-regulated kinase (ERK) is a pivotal kinase in the pathway downstream of Ras, Raf, and MEK, acting as a central link between multiple signaling pathways. We have recently reported the discovery of pyrazolylpyrroles as nanomolar selective ERK inhibitors.[6] Herein we describe our efforts that combine X-ray crystallography, molecular modeling, and medicinal chemistry toward discovery and optimization of pyrimidylpyrroles, a novel series of potent, selective, and orally bioavailable ERK inhibitors.

Despite the encouraging kinase selectivity profile of **1** (Figure 1), the key shortcoming of the pyrazolylpyrrole series remained its insufficient cellular activity ($IC_{50} = 0.54\ \mu M$ for **1** in the Colo205 cell proliferation assay).[6] We chose to search for alternative hinge binding moieties to replace the pyrazole of **1** and prepared a series of aminopyrimidine-based analogues. The aminopyrimidine library culminated in the discovery of **2**, a potent pyrimidylpyrrole ERK inhibitor ($K_I < 2$ nM) possessing improved cellular activity ($IC_{50} =$ 29 nM in the HT29 cell proliferation assay). Unfortunately, the increased cellular potency was accompanied by a significantly degraded selectivity profile. The three kinases affected the most were glycogen synthase kinase 3 (GSK3), cyclin-dependent kinase 2 (CDK2), and AuroraA, with K_I values in the 7−15 nM range (Table 1). This selectivity profile compared unfavorably with that of **1**, which produced K_I values of $3.3\ \mu M$ for GSK3 and $> 4\ \mu M$ for both CDK2 and AuroraA.[6] We initiated crystallographic studies of **2** in order to further our structural understanding of the key binding elements responsible for its ERK inhibition relative to the previously described pyrazolylpyrrole series exemplified by **1**.

Results and Discussion

The resulting X-ray structure (Figure 2) confirmed that the aminopyrimidine fragment of **2** was critical to its activity, making two hydrogen bonds to the hinge region of ERK. Importantly, while the pyrazole ring in **1** engaged the main chain carbonyl of Asp104 in addition to the amide NH of Met106, the aminopyrimidine of **2** formed the second hydrogen bond to the main chain carbonyl of Met106. The former orientation is incompatible with **2**, since it would result in a clash between the gatekeeper Gln103 side chain and the *N*-phenyl fragment of **2**. However, the most surprising aspect of the X-ray structure was the location of the pyrrole linker in **2** relative to **1**. The pyrrole NH is no longer involved in a hydrogen bond with the amide oxygen of the gatekeeper residue Gln103, as observed for **1**. In fact, the pyrrole of **2** is flipped nearly 180° relative to **1**, with the NH proton pointing toward solvent. The gatekeeper residue plays a well-established role in determining the selectivity of kinase inhibitors. The gatekeeper residue in GSK3 and AuroraA is Leu, while the corresponding residue in CDK2 is Phe. The activity of **2** increased by over 250-fold against these three targets compared to **1**. We believe that the degraded selectivity observed for **2** is the result of the loss of gatekeeper recognition function. The amide portion of **2** is making interactions similar to those seen earlier for **1**. The amide carbonyl of **2** forms a hydrogen bond with the catalytic Lys52, and the phenylglycinol motif makes a hydrophobic interaction with the glycine-rich loop.

†The atomic coordinates for ERK2 and GSK3 complexes have been deposited in the Protein Data Bank under accession numbers 3I5Z, 3I60, and 3I4B.

*To whom correspondence should be addressed. Telephone: (617) 444-6100. Fax: 617-444-7822. E-mail: alex_aronov@vrtx.com.

[a] Abbreviations: CDK2, cyclin-dependent kinase 2; EDCI, *N*-ethyl-*N*′-(3-dimethylaminopropyl)carbodiimide; ERK, extracellular signal-regulated kinase; GSK3, glycogen synthase kinase 3.

 Published on Web 09/22/2009

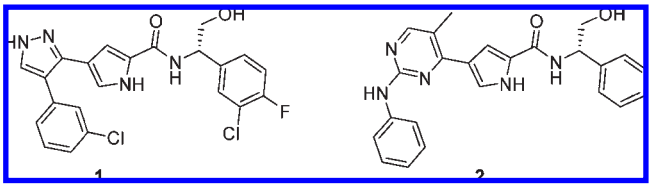

Figure 1. Structures of ERK2 pyrazolylpyrrole inhibitor **1** and lead compound **2**.

Table 1. Effect of the Ortho-Substitution on Selectivity of Pyrimidylpyrroles[a]

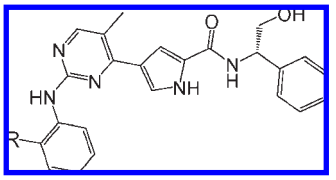

compd	R	ERK2 K_I, nM	GSK3 K_I, nM	CDK2 K_I, nM	AURA K_I, nM	HT29 IC_{50}, nM
2	H	< 2	7	16	15	29
9a	Cl	< 2	190	240	1550	ND
9b	Me	< 2	330	140	860	ND
9c	Et	3	760	210	1430	66
9d	F	< 2	45	57	160	26
9e	CF_3	4	2300	> 4000	> 800	6300
9f	OH	4	< 2	< 100	99	3000

[a] ND: not determined.

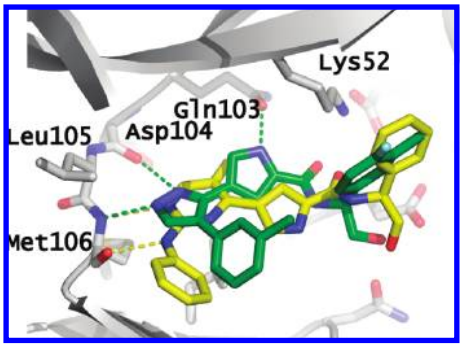

Figure 2. Comparison of ligand orientations of **1** and **2** bound to ERK2.

Pyrimidylpyrroles were prepared as described in Scheme 1. Starting with commercially available trichloroacetylpyrrole, Friedel−Crafts acylation produced diketone **3**. The activated trichloromethylketone was converted to the corresponding ester **4** using sodium methoxide. Pyrrole ring of ester **4** was protected with the tosyl protecting group. Treatment of **5** with dimethylformamide di-*tert*-butylacetal followed by cyclization with the appropriate arylguanidine **12** and subsequent hydrolysis afforded carboxylic acid **8**. Amide coupling with *N*-ethyl-*N*′-(3-dimethylaminopropyl)carbodiimide (EDCI) furnished the desired analogues **9**−**11**.

To enable rational design of ERK selectivity for **2**, we chose to study its binding conformation in GSK3. We have previously reported the X-ray structure of GSK3,[7] and the available construct allowed for efficient ligand crystallization. The orientation of **2** bound to GSK3 is essentially identical to that seen in ERK (Figure 3A). The notable difference is the conformation of the phenylaminopyrimidine; the aniline is in the plane of the aminopyridine in GSK3, while in ERK the phenyl ring is twisted out of plane by 39°. This observation may be attributed to two factors: the size difference between the proximal hinge Tyr134 residue in GSK3 and its Leu105 counterpart in ERK, and the conformation differences of the hinge backbones. The larger aromatic side chain of Tyr134 appears to impart coplanarity on the aniline portion of **2**. Such preference was less pronounced when Tyr134 side chain was replaced with leucine. In addition, the tighter hinge turn seen in ERK results in the placement of the main chain carbonyl of Glu107 approximately 1 Å closer to the ligand relative to the corresponding Pro136 of GSK3, thus favoring a "twisted" conformation observed in ERK. Modeling predicted that introducing an ortho-substituent into the aniline ring would help stabilize the "twisted" conformation of **2** in ERK and destabilize the in-plane GSK-bound conformation. Small substituents (**9a**−**d**, Table 1) were effective at maintaining ERK inhibition and ablating antitarget activity. For instance, 2-chloro substituent (**9a**) provided a 27-fold reduction in GSK3 activity along with 15-fold drop in CDK2 and 100-fold decrease in AuroraA activity, two other kinases in which Leu105 is replaced by aromatic residues, Phe82 in CDK2 and Tyr212 in AuroraA. The smallest substituent, 2-fluoro (**9d**), was least effective because of a less pronounced effect on the aniline torsion angle. A larger 2-CF_3 substituent (**9e**) essentially removed GSK3, CDK2, and AuroraA activity but lost cellular activity. 2-Hydroxy substituent (**9f**) tended to lose both cellular activity and selectivity except in the case of GSK3, in which the hydroxyl likely engages the side chain phenol of Tyr134. To confirm the stabilized out of plane conformation induced by the ortho-substituent, we obtained the X-ray structure of ERK-bound **9a**. Indeed, the ortho-substitution is compatible with the ERK active site, as both K_I and the bound conformation were unchanged upon going from **2** to **9a** (Figure 3B). Addition of the *o*-chloro substituent in **9a** is incompatible with the planar GSK3-bound structure of **2**, as the chlorine would clash with the main chain carbonyl of hinge Val135. The twisted conformation of **9a** as bound to ERK can be expected to position the chlorine within 2.6 Å of the Tyr134 side chain, and it is this detrimental interaction that likely accounts for a dramatic drop on potency against GSK3 and related kinases seen for **9a**.

Another potential selectivity opportunity was located in the phenylglycinol portion of the molecule. The (*S*)-stereochemistry was strongly preferred for phenylglycinol, as **10a** (Table 2) lost over 300-fold in ERK affinity. Preparation of 3-substituted (*S*)-phenylglycinols **10b**−**d** was prompted by comparing the structures of **1** and **2** and led to a 10- to 100-fold separation between ERK and other kinases, likely exploiting the differential flexibility of glycine-rich loop regions. Again, 3-fluoro (**10b**) was too small to effectively engage the ERK glycine-rich loop in a selective fashion.

We proceeded to combine the substitutions to both the aniline and the phenylglycinol to capitalize on the anticipated additive effect of these changes. Indeed, while 2-substituted anilines were most efficient at removing AuroraA activity, the 3-substituted phenylglycinols were only modestly selective against AuroraA. The 3-chloro derivative **10c** was chosen as the reference to study combined substitutions because of its selectivity against GSK3 and CDK2, as well as potent cellular activity (HT29 IC_{50} = 100 nM). As shown in Table 3, the selectivity against AuroraA was improved significantly for most compounds, while GSK3 and CDK2 selectivity margins were also acceptable. Surprisingly, **11a** showed strong inhibition of GSK3, in contrast to closely related **9b** and **10c**. Larger aniline substituents, e.g., **11i** and **11l**, were typically somewhat detrimental to ERK activity; however, most combinations produced selective ERK inhibitors with sub-100 nM cellular potency.

Scheme 1[a]

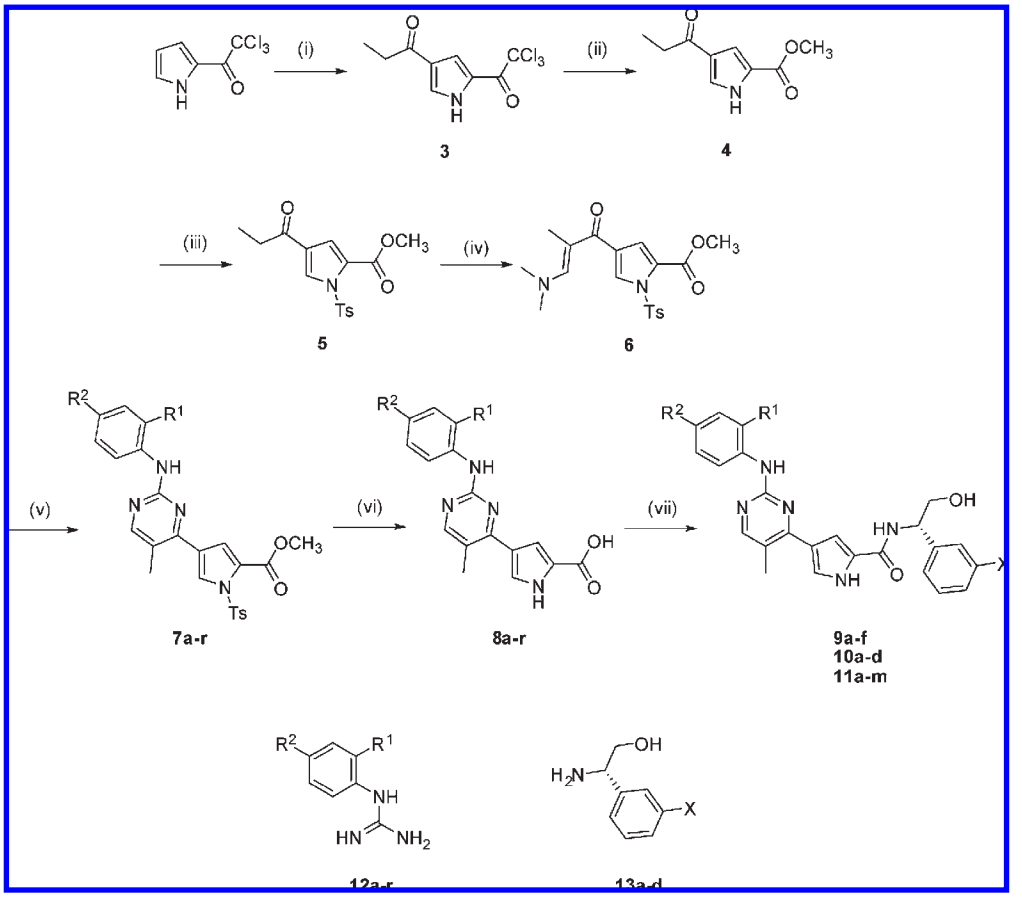

[a] Reagents: (i) CH_3CH_2COCl, $AlCl_3$, CH_2Cl_2; (ii) NaOMe, MeOH; (iii) TsCl, DMAP, CH_2Cl_2, rt, 2 h (iv) $Me_2NHC(O^tBu)_2$, toluene; (v) **12**, toluene, reflux 20 h; (vi) LiOH, H_2O, THF; (vii) **13**, EDCI, HOBt, NMP.

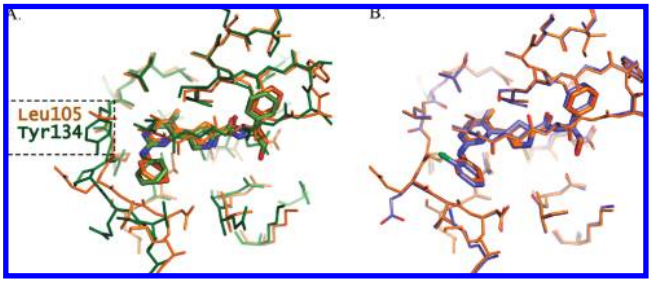

Figure 3. Structural characterization of the binding of pyrimidylpyrroles to kinases: (A) crystal structures of **2** bound to ERK2 (orange) and GSK3 (green); (B) crystal structures of **2** (orange) and **9a** (blue) bound to ERK2.

Compound **11e** was chosen for further studies because of its superior potency and selectivity profile. The extensive counterscreening profile of **11e** is shown in Table S1. It is over 200-fold selective against GSK3, CDK2, and AuroraA and > 500-fold selective against other kinases tested. In addition, **11e** is active in the HT29 cell proliferation assay ($IC_{50} = 48$ nM) and was found to be orally bioavailable in both rat ($F = 65\%$; $t_{1/2} = 3$ h) and mouse ($F = 67\%$; $t_{1/2} = 4.4$ h). A more complete PK profile for **11e** can be found in Supporting Information.

Conclusion

We have designed a series of potent, selective, and orally bioavailable inhibitors of ERK2 kinase starting with a potent, but nonselective, lead compound **2**, followed by several rounds of structure-guided optimization. In particular, the specificity for ERK was optimized following the discovery of a conformational change for **2** when bound to ERK2 relative to antitarget GSK3. Stabilizing the ERK-bound conformation of **2** by introducing additional functionality, we were able to design **11e**, a selective subnanomolar ERK2 inhibitor with potent cellular activity.

This study highlights the utility of rigorous crystallographic studies in multiple kinases to selectivity design. In our experience,

Table 2. Effect of the (*S*)-Phenylglycinol Substitution on Selectivity of Pyrimidylpyrroles[a]

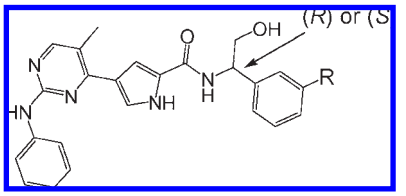

compd	R/ stereo	ERK2 K_I, nM	GSK3 K_I, nM	CDK2 K_I, nM	AURA K_I, nM	HT29 IC_{50}, nM
2	H/(*S*)	;2	7	16	15	29
10a	H/(*R*)	670	540	1100	270	ND
10b	F/(*S*)	< 2	5	ND	ND	ND
10c	Cl/(*S*)	< 2	140	290	19	100
10d	Me/(*S*)	< 2	26	69	45	40

[a] ND: not determined.

Table 3. Relationship between Structure and Kinase Selectivity of Substituted Pyrimidylpyrroles[a]

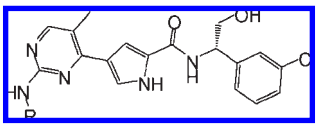

Compound	R_i	ERK2 K_i, nM	GSK3 K_i, nM	CDK2 K_i, nM	AURA K_i, nM	HT29 IC_{50}, nM
10c		< 2	140	290	19	100
11a		< 2	< 2	ND	400	ND
11b		< 2	110	41	440	55
11c		34	1260	150	410	56
11d		5	1100	76	410	98
11e		< 2	395	852	540	48
11f		5	450	316	540	97
11g		< 2	150	410	720	39
11h		< 2	350	642	550	250
11i		13	667	250	280	420
11j		< 2	33	209	15	58
11k		< 2	310	170	> 800	280
11l		15	45	138	11	58
11m		3	> 2500	> 2500	> 200	230

[a] ND: not determined.

observations of seemingly small ligand conformational changes that occur upon binding to kinases have provided invaluable guidance for addressing the kinase selectivity problem.

Experimental Section

General Experimental Details. All commercial reagents and anhydrous solvents were obtained from commercial sources and were used without further purification, unless otherwise specified. Mass samples were analyzed on a MicroMass ZQ, ZMD, Quattro LC, or Quatro II mass spectrometer operated in a single MS mode with electrospray ionization. Samples were introduced into the mass spectrometer using flow injection (FIA) or chromatography. The mobile phase for all mass analysis consisted of acetonitrile−water mixtures with either 0.2% formic acid or 5 mM ammonium formate (pH 7). High resolution mass spectra were measured using a 9.4 T APEX III FTMS Bruker Daltonics instrument. The following HPLC methods were used to obtain the reported retention times: (i) Method A: YMC Pro18 column, 50 mm × 4.6 mm; linear gradient from 10% to 90% CH_3CN in H_2O over 5 min; flow rate 0.8 mL/min. (ii) Method B: Waters Symmetry C18 column, 4.6 mm × 50 mm; linear gradient from 10% to 90% CH_3CN in H_2O over 3 min (0.2% formic acid); flow rate 1.5 mL/min. (iii) Method C: Water symmetry C18 column, 4.6 mm × 50 mm; linear gradient from 2% to 90% CH_3CN in H_2O over 3 min (2% ammonium formate); flow rate 1.5 mL/min; detection diode array. ^{1}H NMR spectra (δ, ppm) was recorded either using a Bruker DRX-500 (500 MHz) or Bruker Avance II-300 (300 MHz) instrument. Elemental analyses were performed by Quantitative Technologies Inc. Column chromatography was performed using Merck silica gel 60 (0.040−0.063 mm). Preparative reverse phase chromatography was carried out using an Agilent Zorbax SB-C18 column, 21.2 mm × 100 mm, a linear gradient from 10% to 90% CH_3CN in H_2O over 10 min (0.1% trifluoroacetic acid), and a flow rate of 20 mL/min. The aryl guanidines **12a**−**r** were synthesized according to published procedures.[8] The substituted phenylglycinols **13b**−**d** were prepared following literature procedures.[9]

The purity of final compounds was assessed on the basis of analytical HPLC, and the results were greater than 95% unless specified otherwise.

Molecular Modeling. Constrained docking studies were performed with Glide, version 3.0,[10] in standard docking mode and used X-ray structures of related ligands as docking templates. The structures were protonated at pH 7. Docked poses were reminimized in MMFF94s[11] force field as implemented in MOE.[12]

Experimental Procedures and Characterization Data for Analogues 2−11. 1-(5-(2,2,2-Trichloroacetyl)-1*H*-pyrrol-3-yl)propan-1-one (3). To a mixture of trichloroacetylpyrrole (50 g, 235 mmol) and $AlCl_3$ (38 g, 289 mmol) in CH_2Cl_2 (20 mL) at −20 °C was added propionyl chloride (290 mmol). The reaction mixture was stirred for 2 h at room temperature and then poured into a mixture of ice and H_2O. The mixture was extracted with diethyl ether. The organic extract was washed with brine, dried over Na_2SO_4, and concentrated under vacuum. The crude product was recrystallized from ethanol to afford an off-white solid (35 g, 60%). ^{1}H NMR (300 MHz, $CDCl_3$) δ 9.82 (s, 1H), 7.75 (d, J = 1.2 Hz, 2H), 2.86 (q, J = 7.3 Hz, 2H), and 1.24 (t, J = 7.3 Hz, 3H) ppm.

Methyl 4-Propionyl-1*H*-pyrrole-2-carboxylate (4). To a stirred solution of 4-propionyl-2-(trichloroacetyl)pyrrole **3** (35.0 g, 140 mmol) in methanol (250 mL) was added a solution of NaOH in methanol (4.37 M, 37 mL, 164.5 mmol) over 10 min. The mixture was stirred for 1 h at room temperature. The mixture was concentrated under reduced pressure. The residue was diluted with diethyl ether and H_2O. The organic layer was separated, washed with H_2O and brine, dried over Na_2SO_4, and concentrated in vacuo to afford the title compound as a white solid (34 g, 95%). ^{1}H NMR (300 MHz, $CDCl_3$) δ 9.45 (br, 1H), 7.42 (d, J = 1.5 Hz, 1H), 7.20 (d, J = 1.5 Hz, 1H), 3.76 (s, 3H), 2.68 (q, J = 7.4 Hz, 2H) and 1.06 (t, J = 7.3 Hz, 3H) ppm.

Methyl 4-Propionyl-1-tosyl-1*H*-pyrrole-2-carboxylate (5). To a solution of the ketone **4** (18.1 g, 100 mmol) in CH_2Cl_2 (100 mL) was added DMAP (1.22 g, 10 mmol) and TsCl (19.1 g, 100 mmol). The solution was stirred for 2 h at room temperature and determined to be complete by HPLC. The solution was diluted with CH_2Cl_2, washed with H_2O and brine, dried over Na_2SO_4, and concentrated in vacuo. The title compound was recovered

as white solid (33.8 g, 95%). ^{1}H NMR (300 MHz, $CDCl_3$) δ 8.27 (d, J = 2.0 Hz, 1H), 7.94 (d, J = 8.4 Hz, 2H), 7.41−7.36 (m, 3H), 3.78 (s, 3H), 2.85 (d, J = 7.3 Hz, 2H), 2.47 (s, 3H), and 1.23 (t, J = 7.3 Hz, 3H) ppm.

Methyl 4-(3-(Dimethylamino)-2-methylacryloyl)-1-tosyl-1*H*-pyrrole-2-carboxylate (6). To a stirred solution of the ketone **5** (9.05 g, 27 mmol) in toluene (90 mL) was added dimethylformamide di-*tert*-butylacetal (9.4 mL, 41 mmol). The reaction mixture was heated for 24 h at 75 °C. The cooled reaction mixture was washed with H_2O twice and concentrated under reduced pressure to provide a brown solid. The solid was triturated with methyl *tert*-butyl ether, and the resulting slurry was filtered, rinsed with methyl *tert*-butyl ether, and dried in a vacuum oven to afford the title compound (8.8 g, 83.5% yield) as an off-white solid. ^{1}H NMR (300 MHz, $CDCl_3$) δ 7.89 (t, J = 8.5 Hz, 2H), 7.87 (s, 1H), 7.34 (d, J = 8.1 Hz, 2H), 7.24−7.19 (m, 2H), 3.76 (s, 3H), 3.14 (s, 6H), 2.45 (s, 3H), and 2.13 (s, 3H) ppm.

Methyl 4-(2-(2,3-Dimethylphenylamino)-5-methylpyrimidin-4-yl)-1-tosyl-1*H*-pyrrole-2-carboxylate (7). To a stirred solution of enaminone **6** (2.0 g, 5.1 mmol) in toluene (20 mL) was added 2,3-dimethylphenylguanidine HCl salt (1.75 g, 8.7 mmol) and *N*,*N*-diisopropylethylamine (1.7 mL, 9.2 mmol). The mixture was heated to reflux for 20 h using a Dean−Stark trap to collect water. The mixture was cooled slightly, and the solvent was removed under reduced pressure. The residue was dissolved in CH_2Cl_2 (10 mL) and MeOH (1 mL), washed with H_2O (×2), dried over Na_2SO_4, filtered, and concentrated under reduced pressure. The residue was purified by column chromatography with gradient 50−100% hexane in EtOAc to provide a mixture of the tosylated and detosylated product (1.6 g, 75% yield).

4-(2-(2,3-Dimethylphenylamino)-5-methylpyrimidin-4-yl)-1-tosyl-1*H*-pyrrole-2-carboxylic Acid (8). To a suspension of ester **7** (1.0 g, 2.2 mmol) in THF (10 mL) and H_2O (10 mL) was added LiOH (230 mg, 5.5 mmol). The reaction mixture was heated at reflux for overnight. The solvent was removed under reduced pressure. The residue was diluted with 4 mL of H_2O and acidified with concentrated HCl to pH 4.5. The resulting solid was collected by vacuum filtration. The filter cake was suspended in 5 mL of H_2O and stirred for 30 min. The solid was collected by vacuum filtration and dried overnight in a vacuum oven at 60 °C to provide the product as an off-white solid (720 mg, 90%). ^{1}H NMR (300 MHz, DMSO-d_6) δ 8.93−8.88 (br, 1H), 8.13 (s, 1H), 7.56 (s, 1H), 7.31 (d, J = 8.2 Hz, 2H), 7.12−7.01 (m, 2H), 2.3 (d, J = 9.7 Hz, 6H), 2.11 (s, 3H).

General Procedure for Preparation of Products 2, 9a−f, 10a−d, and 11a−m. To a mixture of the acid **8** (1.0 mmol), 1-(3-dimethylaminopropyl)-3-ethylcarbodimide hydrochloride (380 mg, 2 mmol), 1-hydroxybenzotriazole (42.8 mg, 0.3 mmol), and 3-chlorophenylglycinol (270 mg, 1.3 mmol) in NMP (4 mL) was added TEA (0.18 mL, 1.3 mmol). The reaction mixture was stirred at room temperature for 90 min and then poured into 8 mL of H_2O. The mixture was stirred for 30 min and then filtered. The filter cake was dried in vacuo and then purified using column chromatography (gradient 0−5% MeOH/CH_2Cl_2) to yield the product.

(*S*)-*N*-(2-Hydroxyl-1-phenylethyl)-4-{5-methyl-2-(phenylamino)-pyrimidin-4-yl}-1*H*-pyrrole-2-carboxamide (2). HPLC (method A) t_R = 4.0 min (>95%). LC−MS (method B) t_R = 2.3 min, m/z = 414.5 [M + H]; (method C) t_R = 2.8 min, 414.3 [M + H]. HRMS calcd for $C_{24}H_{24}N_5O_2$ 414.192 45, found 414.192 85. ^{1}H NMR (300 MHz, DMSO-d_6) δ 9.23 (s, 1H), 8.49 (d, J = 8.2 Hz, 1H), 8.25 (s, 1H), 7.82 (d, J = 8.2 Hz, 2H), 7.60 (s, 1H), 7.55 (s, 1H), 7.42−7.21 (m, 7H), 6.91 (t, J = 7.3 Hz, 1H), 5.08 (t, J = 7.3 Hz, 1H), 4.92 (t, J = 5.7 Hz, 1H), 3.70 (t, J = 5.8 Hz, 2H), and 2.36 (s, 3H) ppm.

(*S*)-4-{2-(2-Chlorophenylamino)-5-methylpyrimidin-4-yl}-*N*-{1-phenyl-2-hydroxyethyl}-1*H*-pyrrole-2-carboxamide (9a). HPLC (method A) t_R = 4.27 min (>95%). LC−MS (method B) t_R = 2.86 min, 448.4 as [M + H] peak; (method C) t_R = 2.45 min, m/z = 448.2 as [M + H] peak. HRMS calcd for $C_{24}H_{23}ClN_5O_2$ 448.153 48, found 448.153 56. ^{1}H NMR (300 MHz, DMSO-d_6) δ 8.51 (d, J = 8.1 Hz, 1H), 8.26−8.19 (m, 2H), 7.60 (s, 1H), 7.51 (t, J = 8.1 Hz, 2H), 7.37 (dd, J = 7.6, 16.9 Hz, 4H), 7.30 (s, 1H), 7.26−7.21 (m, 1H), 7.09 (t, J = 7.6 Hz, 1H), 5.13−5.02 (m, 1H), 3.70−3.64 (m, 2H), 2.50 (t, J = 1.7 Hz, 3H) ppm.

(*S*)-4-{2-(2-Methylphenylamino)-5-methylpyrimidin-4-yl}-*N*-{1-phenyl-2-hydroxyethyl}-1*H*-pyrrole-2-carboxamide (9b). HPLC (method A) t_R = 4.0 min (>95%). LC−MS (method B) t_R = 2.11 min, m/z = 428.5 as [M + H] peak; (method C) t_R = 2.86 min, m/z = 428.32 as [M + H] peak. HRMS calcd for $C_{25}H_{26}N_5O_2$ 428.208 10, found 428.209 03.

(*S*)-4-{2-(2-Ethylphenylamino)-5-methylpyrimidin-4-yl}-*N*-{1-phenyl-2-hydroxyethyl}-1*H*-pyrrole-2-carboxamide (9c). HPLC (method A) t_R = 4.16 min (>95%). LC−MS (method B) t_R = 2.2 min, m/z = 442.5 as [M + H] peak; (method C) t_R = 2.99 min, m/z = 442.31 as [M + H] peak. HRMS calcd for $C_{24}H_{23}ClN_5O_2$ 448.153 48, found 448.153 56. ^{1}H NMR (300 MHz, DMSO-d_6) δ 8.73−8.68 (m, 1H), 8.59−8.53 (m, 1H), 8.13 (s, 1H), 7.58−7.52 (m, 3H), 7.40−7.11 (m, 8H), 5.18−5.04 (m, 1H), 3.72−3.67 (m, 2H), 2.73 (m, 2H), 2.20 (s, 3H), and 1.13 (t, J = 7.5 Hz, 3H) ppm

(*S*)-4-{2-(2-Fluorophenylamino)-5-methylpyrimidin-4-yl}-*N*-{1-phenyl-2-hydroxyethyl}-1*H*-pyrrole-2-carboxamide (9d). HPLC (method A) t_R = 4.1 min (>95%). LC−MS (method B) t_R = 2.56 min, m/z = 432.5 as [M + H] peak; (method C) t_R = 2.91 min, m/z = 432.21 as [M + H] peak. HRMS calcd for $C_{24}H_{23}FN_5O_2$ 432.183 03, found 432.182 14. ^{1}H NMR (300 MHz, DMSO-d_6) δ 8.61 (s, 1H), 8.48 (d, J = 8.1 Hz, 1H), 8.23 (s, 1H), 8.02 (t, J = 8.0 Hz, 1H), 7.58 (s, 1H), 7.52 (s, 1H), 7.36 (dd, J = 7.6, 24.3 Hz, 4H), 7.26−7.15 (m, 3H), 7.07 (t, J = 6.4 Hz, 1H), 5.16−5.04 (m, 1H), 3.74−3.68 (m, 2H), and 2.37 (s, 3H) ppm.

(*S*)-4-{2-(2-Trifluoromethylphenylamino)-5-methylpyrimidin-4-yl}-*N*-{1-phenyl-2-hydroxyethyl}-1*H*-pyrrole-2-carboxamide (9e). HPLC (method A) t_R = 4.35 min (>95%). LC−MS (method B) t_R = 2.8 min, m/z = 482.5 as [M + H] peak; (method C) t_R = 3.12 min, m/z = 482.01 as [M + H] peak. HRMS calcd for $C_{25}H_{23}F_3N_5O_2$ 482.179 84, found 482.179 99. ^{1}H NMR (300 MHz, DMSO-d_6) δ 8.55 (d, J = 8.5 Hz, 1H), 8.31 (s, 1H), 8.19 (s, 1H), 7.97 (d, J = 8.3 Hz, 1H), 7.71 (q, J = 7.6 Hz, 2H), 7.58 (s, 1H), 7.50 (s, 1H), 7.24−7.37 (m, 6H), 5.08 (d, J = 7.0 Hz, 1H), 3.68 (d, J = 5.6 Hz, 2H), and 2.36 (s, 3H) ppm.

(*S*)-4-{2-(2-Hydroxyphenylamino)-5-methylpyrimidin-4-yl}-*N*-{1-phenyl-2-hydroxyethyl}-1*H*-pyrrole-2-carboxamide (9f). HPLC (method A) t_R = 3.75 min (>95%). LC−MS (method B) t_R = 2.1 min, m/z = 430.5 as [M + H] peak; (method C) t_R = 2.1 min, m/z = 430.47 as [M + H] peak. HRMS calcd for $C_{24}H_{24}N_5O_3$ 430.187 37, found 430.186 37.

(*R*)-*N*-(2-Hydroxyl-1-phenylethyl)-4-{5-methyl-2-(phenylamino)-pyrimidin-4-yl}-1*H*-pyrrole-2-carboxamide (10a). HPLC (method A) t_R = 4.0 min (>95%). LC−MS (method B) t_R = 2.3 min, m/z = 414.5 as [M + H] peak; (method C) t_R = 2.8 min, m/z = 414.3 as [M + H] peak. HRMS calcd for $C_{24}H_{24}N_5O_2$ 414.192 45, found 414.192 05.

(*S*)-*N*-{1-(3-Fluorophenyl)-2-hydroxyethyl}-4-{5-methyl-2-(phenylamino)pyrimidin-4-yl}-1*H*-pyrrole-2-carboxamide (10b). HPLC (method A) t_R = 4.16 min (>95%). LC−MS (method B) t_R = 2.4 min, m/z = 432.5 as [M + H] peak; (method C) t_R = 2.51 min, m/z = 432.33 as [M + H] peak. HRMS calcd for $C_{24}H_{23}FN_5O_2$ 432.183 03, found 432.183 44.

(*S*)-*N*-{1-(3-Chlorophenyl)-2-hydroxyethyl}-4-{5-methyl-2-(phenylamino)pyrimidin-4-yl}-1*H*-pyrrole-2-carboxamide (10c). HPLC (method A) t_R = 4.31 min (>95%). LC−MS (method B) t_R = 2.52 min, m/z = 448.5 as [M + H] peak; (method C) t_R = 2.7 min, m/z = 448.2 as [M + H] peak. HRMS calcd for $C_{24}H_{23}ClN_5O_2$ 448.153 48, found 448.154 77.

(S)-*N*-{1-(3-Methylphenyl)-2-hydroxyethyl}-4-{5-methyl-2-(phenylamino)pyrimidin-4-yl}-1*H*-pyrrole-2-carboxamide (10d). HPLC (method A) t_R = 4.25 min (>95%). LC−MS (method

B) t_R = 2.5 min, m/z = 428.6 as [M + H] peak; (method C) t_R = 2.95 min, m/z = 428.02 as [M + H] peak. HRMS calcd for $C_{25}H_{26}N_5O_2$ 428.208 10, found 428.208 22.

(*S*)-4-{2-(2-Methylphenylamino)-5-methylpyrimidin-4-yl}-*N*-{1-(3-chlorophenyl)-2-hydroxyethyl}-1*H*-pyrrole-2-carboxamide (11a). HPLC (method A) t_R = 4.29 min (>95%). LC−MS (method B) t_R = 2.3 min, m/z = 462.5 [M + H], 460.4 [M − H]; (method C) t_R = 3.0 min, m/z = 462.23 [M + H]. HRMS calcd for $C_{25}H_{25}ClN_5O_2$ 462.169 13, found 462.169 78. ^{1}H NMR (300 MHz, DMSO-d_6) δ 8.72 (s, 1H), 8.58 (d, J = 8.2 Hz, 1H), 8.16 (s, 1H), 7.65−7.58 (m, 2H), 7.53 (s, 1H), 7.46 (s, 1H), 7.38−7.19 (m, 4H), 7.07 (t, J = 7.3 Hz, 1H), 5.10−5.03 (m, 1H), 3.68 (d, J = 6.1 Hz, 2H), 2.36 (s, 3H), and 2.25 (s, 3H) ppm.

(*S*)-4-{2-(2,3-Dimethylphenylamino)-5-methylpyrimidin-4-yl}-*N*-{1-(3-chlorophenyl)-2-hydroxyethyl}-1*H*-pyrrole-2-carboxamide (11b). HPLC (method A) t_R = 4.42 min (>95%). LC−MS (method B) t_R = 2.3 min, m/z = 476.5 [M + H], m/z = 474.4 [M − H]; (method C) t_R = 2.3 min, m/z = 476.21 [M + H]. HRMS calcd for $C_{26}H_{27}ClN_5O_2$ 476.184 78, found 476.185 07.

(*S*)-4-{2-(3-Fluoro-2-methylphenylamino)-5-methylpyrimidin-4-yl}-*N*-{1-(3-chlorophenyl)-2-hydroxyethyl}-1*H*-pyrrole-2-carboxamide (11c). HPLC (method A) t_R = 4.4 min (>95%). LC−MS (method B) t_R = 2.6 min, m/z = 480.4 [M + H], m/z = 478.4 [M − H]; (method C) t_R = 2.69 min, m/z = 480.29 [M + H]. HRMS calcd for $C_{25}H_{24}ClFN_5O_2$ 480.159 71, found 480.160 35. ^{1}H NMR (300 MHz, DMSO-d_6) δ 8.74 (s, 1H), 8.56 (d, J = 8.3 Hz, 1H), 8.19 (s, 1H), 7.57−7.46 (m, 3H), 7.40−7.30 (m, 2H), 7.21 (dd, J = 8.1, 15.1 Hz, 3H), 6.93 (t, J = 9.0 Hz, 1H), 5.07 (dd, J = 6.6, 14.4 Hz, 1H), 3.73−3.67 (m, 2H), 2.42 (s, 3H), and 2.07 (s, 3H) ppm.

(*S*)-4-{2-(4-Chloro-2-methylphenylamino)-5-methylpyrimidin-4-yl}-*N*-{1-(3-chlorophenyl)-2-hydroxyethyl}-1*H*-pyrrole-2-carboxamide (11d). HPLC (method A) t_R = 4.59 min (>95%). LC−MS (method B) t_R = 2.81 min, m/z = 496.4 [M + H], m/z = 494.4 [M-H]; (method C) t_R = 2.99 min, m/z = 496.31 [M + H]. HRMS calcd for $C_{25}H_{24}Cl_2N_5O_2$ 496.130 16, found 496.130 18. ^{1}H NMR (300 MHz, DMSO-d_6) δ 8.64 (d, J = 8.8 Hz, 1H), 8.57 (d, J = 8.1 Hz, 1H), 8.18 (s, 1H), 7.71 (d, J = 8.9 Hz, 1H), 7.56 (s, 1H), 7.52 (s, 1H), 7.44 (d, J = 11.8 Hz, 1H), 7.24−7.35 (m, 5H), 5.07 (d, J = 6.6 Hz, 1H), 3.68 (d, J = 6.2 Hz, 2H), 2.36 (s, 3H), and 2.25 (s, 3H) ppm.

4-[2-(2-Chloro-4-fluorophenylamino)-5-methylpyrimidin-4-yl]-1-toluene-4-sulfonyl)pyrrole-2-carboxylic Acid [1-(3-Chlorophenyl)-2-hydroxyethyl]amide (11e). HPLC (method A) t_R = 4.43 min (>95%). LC−MS (method B) t_R = 3.26 min, m/z = 500.34 as [M + H] peak. HRMS calcd for $C_{24}H_{21}Cl_2FN_5O_2$ 500.105 08, found 500.105 86. ^{1}H NMR (300 MHz, DMSO-d_6) δ 8.52 (d, J = 8.4 Hz, 1H), 8.23 (d, J = 11.0 Hz, 2H), 8.03 (dd, J = 5.9, 9.0 Hz, 1H), 7.57 (s, 1H), 7.48 (dd, J = 2.7, 8.6 Hz, 2H), 7.37−7.20 (m, 5H), 5.09−4.96 (m, 2H), 3.72 (s, 2H), and 2.35 (s, 3H) ppm.

(*S*)-4-{2-(4-Chloro-2-fluorophenylamino)-5-methylpyrimidin-4-yl}-*N*-{1-(3-chlorophenyl)-2-hydroxyethyl}-1*H*-pyrrole-2-carboxamide (11f). HPLC (method A) t_R = 4.89 min (>95%). LC−MS (method B) t_R = 3.25 min, m/z = 500.4 [M + H], m/z = 498.4 [M − H]; (method C) t_R = 2.81 min, m/z = 500.33 [M + H]. HRMS calcd for $C_{24}H_{21}Cl_2FN_5O_2$ 500.105 08, found 500.106 51. ^{1}H NMR (300 MHz, DMSO-d_6) δ 8.81 (s, 1H), 8.56 (d, J = 8.3 Hz, 1H), 8.25 (s, 1H), 8.07 (t, J = 8.8 Hz, 1H), 7.61 (d, J = 11.6 Hz, 1H), 7.53 (s, 1H), 7.45 (dd, J = 2.4, 11.2 Hz, 1H), 7.36−7.25 (m, 5H), 5.11−5.04 (m, 1H), 3.68 (d, J = 5.6 Hz, 2H), and 2.37 (s, 3H) ppm.

(*S*)-4-{2-(2-Ethylphenylamino)-5-methylpyrimidin-4-yl}-*N*-{1-(3-chlorophenyl)-2-hydroxyethyl}-1*H*-pyrrole-2-carboxamide (11g). HPLC (method A) t_R = 4.44 min (>95%). LC−MS (method B) t_R = 2.4 min, m/z = 476.5 [M + H], m/z = 474.4 [M − H]; (method C) t_R = 2.47 min, m/z = 476.26 [M + H]. HRMS calcd for $C_{26}H_{27}ClN_5O_2$ 476.184 78, found 476.185 17. ^{1}H NMR (300 MHz, DMSO-d_6) δ 8.83 (s, 1H), 8.60 (d, J = 8.1 Hz, 1H), 8.13 (s, 1H), 7.57 (d, J = 9.3 Hz, 1H), 7.46 (s, 1H), 7.40−7.13 (m, 8H), 5.08−5.04 (m, 1H), 3.68 (d, J = 6.1 Hz, 2H), 2.64 (q, J = 7.5 Hz, 2H), 2.36 (s, 3H), 1.13 (t, J = 7.5 Hz, 3H) ppm.

(*S*)-*N*-{1-(3-Chlorophenyl)-2-hydroxyethyl}-4-{2-(2,3-dihydro-1*H*-inden-4-ylamino)-5-methylpyrimidin-4-yl}-1*H*-pyrrole-2-carboxamide (11h). HPLC (method A) t_R = 4.59 min (>95%). LC−MS (method B) t_R = 2.65 min, m/z = 488.5 [M + H], m/z = 486.4 [M − H]; (method C) t_R = 2.73 min, m/z = 488.26 [M + H]. HRMS calcd for $C_{27}H_{27}ClN_5O_2$ 488.184 78, found 488.184 89. ^{1}H NMR (300 MHz, DMSO-d_6) d 8.64 (s, 1H), 8.54 (d, J = 8.6 Hz, 1H), 8.20 (s, 1H), 7.64−7.56 (m, 2H), 7.46 (s, 1H), 7.34 (t, J = 4.3 Hz, 3H), 7.12 (q, J = 7.7 Hz, 2H), 6.98 (d, J = 7.0 Hz, 1H), 5.08 (t, J = 7.2 Hz, 1H), 3.69 (d, J = 6.3 Hz, 2H), 2.94−2.78 (m, 4H), 2.35 (d, J = 12.4 Hz, 3H), and 2.01 (dd, J = 7.6, 14.8 Hz, 2H) ppm.

(*S*)-*N*-{1-(3-Chlorophenyl)-2-hydroxyethyl}-4-{5-methyl-2(5,6,7,8-tetrhydronaphthalen-1-ylamino)pyrimidin-4-yl}-1*H*-pyrrole-2-carboxamide (11i). HPLC (method A) t_R = 4.66 min (>95%). LC−MS (method B) t_R = 2.56 min, m/z = 502.5 [M + H], m/z = 500.4 [M − H]; (method C) t_R = 3.38 min, m/z = 502.34 [M + H]. HRMS calcd for $C_{28}H_{29}ClN_5O_2$ 502.200 43, found 502.201 10.

(*S*)-4-{2-(Benzo[*d*]1,3-dioxolylamino)-5-methylpyrimidin-4-yl}-*N*-{1-(3-chlorophenyl)-2-hydroxyethyl}-1*H*-pyrrole-2-carboxamide (11j). HPLC (method A) t_R = 4.27 min (>95%). LC−MS (method B) t_R = 2.37 min, m/z = 492.5 [M + H], m/z = 490.4 [M − H]; (method C) t_R = 2.39 min, m/z = 492.24 [M + H]. HRMS calcd for $C_{25}H_{23}ClN_5O_4$ 492.143 31, found 492.143 94.

(*S*)-*N*-{1-(3-Chlorophenyl)-2-hydroxyethyl}-4-{2-(2,2-difluorobenzo[*d*][1,3]dioxol-4-ylamino)-5-methylpyrimidin-4-yl}-1*H*-pyrrole-2-carboxamide (11k). HPLC (method A) t_R = 4.84 min (>95%). LC−MS (method B) t_R = 3.1 min, m/z = 528.5 [M + H], m/z = 526.4 [M − H]; (method C) t_R = 3.17 min, m/z = 528.17 [M + H]. HRMS calcd for $C_{25}H_{21}ClF_2N_5O_4$ 528.124 46, found 528.125 83.

(*S*)-*N*-{1-(3-Chlorophenyl)-2-hydroxyethyl}-4-{2-(2,3-dihydrobenzo[*b*][1,4]dioxin-5-ylamino)-5-methylpyrimidin-4-yl}-1*H*-pyrrole-2-carboxamide (11l). HPLC (method A) t_R = 4.31 min (>95%). LC−MS (method B) t_R = 2.34 min, m/z = 506.5 [M + H], m/z = 504.4 [M − H]; (method C) t_R = 2.91 min, m/z = 506.15 [M + H]. HRMS calcd for $C_{26}H_{25}ClN_5O_4$ 506.158 96, found 506.159 65.

(*S*)-4-{2-(2,3-Dimethylphenylamino)-5-methylpyrimidin-4-yl}-*N*-{1-(3-chlorophenyl)-2-hydroxyethyl}-1*H*-pyrrole-2-carboxamide (11m). HPLC (method A) t_R = 4.38 min (>95%). LC−MS (method B) t_R = 2.7 min, m/z = 508.5 [M + H], m/z = 506.4 [M − H] (method C) t_R = 3.08 min, m/z = 508.22 [M + H]. HRMS calcd for $C_{26}H_{27}ClN_5O_4$ 508.174 61, found 508.173 66.

Supporting Information Available: Biochemical and biological procedures, crystallization conditions, and data collection statistics. This material is available free of charge via the Internet at http://pubs.acs.org.

References

(1) Sebolt-Leopold, J. S.; Herrera, R. Targeting the mitogen-activated protein kinase cascade to treat cancer. *Nat. Rev. Cancer* **2004**, *4*, 937–947.
(2) Smalley, K. S. A pivotal role for ERK in the oncogenic behaviour of malignant melanoma? *Int. J. Cancer* **2003**, *104*, 527–532.
(3) Kohno, M.; Pouyssegur, J. Pharmacological inhibitors of the ERK signaling pathway: application as anticancer drugs. *Prog. Cell Cycle Res.* **2003**, *5*, 219–224.
(4) Chang, F.; Steelman, L. S.; Shelton, J. G.; Lee, J. T.; Navolanic, P. M.; Blalock, W. L.; Franklin, R.; McCubrey, J. A. Regulation of cell cycle progression and apoptosis by the Ras/Raf/MEK/ERK pathway (review). *Int. J. Oncol.* **2003**, *22*, 469–480.
(5) Hilger, R. A.; Scheulen, M. E.; Strumberg, D. The Ras-Raf-MEK-ERK pathway in the treatment of cancer. *Onkologie* **2002**, *25*, 511–518.
(6) Aronov, A. M.; Baker, C.; Bemis, G. W.; Cao, J.; Chen, G.; Ford, P. J.; Germann, U. A.; Green, J.; Hale, M. R.; Jacobs, M.; Janetka,

J. W.; Maltais, F.; Martinez-Botella, G.; Namchuk, M. N.; Straub, J.; Tang, Q.; Xie, X. Flipped out: structure-guided design of selective pyrazolylpyrrole ERK inhibitors. *J. Med. Chem*. **2007**, *50*, 1280–1287.
(7) ter Haar, E.; Coll, J. T.; Austen, D. A.; Hsiao, H. M.; Swenson, L.; Jain, J. Structure of GSK3beta reveals a primed phosphorylation mechanism. *Nat. Struct. Biol*. **2001**, *8*, 593–596.
(8) Moon, Y.-C.; Green, J.; Davis, R.; Choquette, D.; Pierce, A.; Ledeboer, M. US2004/9996, **2004**.
(9) Barrow, J. C.; Ngo, P. L.; Pellicore, J. M.; Selnick, H. G.; Nantermet, P. G. A facile three-step synthesis of 1,2-amino alcohols using the Ellman homochiral *tert*-butylsulfinamide. *Tetrahedron Lett*. **2001**, *42*, 2051–2054.
(10) (a) Friesner, R. A.; Banks, J. L.; Murphy, R. B.; Halgren, T. A.; Klicic, J. J.; Mainz, D. T.; Repasky, M. P.; Knoll, E. H.; Shelley, M.; Perry, J. K.; Shaw, D. E.; Francis, P.; Shenkin, P. S. Glide: a new approach for rapid, accurate docking and scoring. 1. Method and assessment of docking accuracy. *J. Med. Chem*. **2004**, *47*, 1739–1749. (b) Halgren, T. A.; Murphy, R. B.; Friesner, R. A.; Beard, H. S.; Frye, L. L.; Pollard, W. T.; Banks, J. L. Glide: a new approach for rapid, accurate docking and scoring. 2. Enrichment factors in database screening. *J. Med. Chem*. **2004**, *47*, 1750–1759.
(11) Halgren, T. A. MMFFVI: MMFF94s option for energy minimization studies. *J. Comput. Chem*. **1999**, *20*, 720–729.
(12) *Molecular Operating Environment*; Chemical Computing Group Inc.: Montreal, Canada, 2005.